mathematics

MDPI

Article

Motion Synchronization Control for a Large Civil Aircraft's Hybrid Actuation System Using Fuzzy Logic-Based Control Techniques

Waheed Ur Rehman [1,2,3,*], Xingjian Wang [3], Zeeshan Hameed [4] and Muhammad Yasir Gul [5]

[1] Department of Mechatronics Engineering, University of Chakwal, Chakwal 48800, Pakistan
[2] Institute of Intelligent Machinery, Faculty of Materials and Manufacturing, Beijing University of Technology, Beijing 100124, China
[3] School of Automation Science and Electrical Engineering, Beihang University, Beijing 100191, China; wangxj@buaa.edu.cn
[4] Faculty of Science and Technology, Free University of Bolzano, 39100 Bolzano, Italy; zeeshan.hameed@natec.unibz.it
[5] Department of Structural Engineering, MCE Risalpur, Risalpur 23200, Pakistan; muyagul.pg19mce@student.nust.edu.pk
* Correspondence: wrehman87@bjut.edu.cn

Abstract: The motion synchronization of the hybrid actuation system (composed of a servo-hydraulic actuator and an electro-mechanical actuator) is very important for all applications, especially for civil aircraft. The current research presents a nested-loop control design technique to synchronize motion between two different actuators, such as a servo-hydraulic actuator (SHA) and an electro-mechanical actuator (EMA). The proposed strategy consists of a trajectory, an intelligent position controller (fuzzy logic-based controller), a feed-forward controller, and an intelligent force controller (fuzzy logic-based controller). Position, speed, and acceleration signals are produced by trajectory at a frequency that both SHA and EMA can follow. The SHA/EMA system's position tracking performance is enhanced by the feed-forward controller and intelligent position controller working together, while the intelligent force tracking controller lowers the issue of force fighting by focusing on the rigid coupling effect. To verify the effectiveness of the proposed strategy, simulations are performed in the Matlab/Simulink environment. The result shows that the proposed intelligent control strategy not only reduces initial force fighting, but also improves load-rejection performance and output-trajectory tracking performance.

Keywords: motion synchronization; electro-mechanical actuator; hydraulic actuator; intelligent control; PID control

MSC: 93C85; 93C42

Citation: Ur Rehman, W.; Wang, X.; Hameed, Z.; Gul, M.Y. Motion Synchronization Control for a Large Civil Aircraft's Hybrid Actuation System Using Fuzzy Logic-Based Control Techniques. *Mathematics* **2023**, *11*, 1576. https://doi.org/10.3390/math11071576

Academic Editors: Fang Liu and Qianyi Liu

Received: 15 February 2023
Revised: 19 March 2023
Accepted: 21 March 2023
Published: 24 March 2023

1. Introduction

One of the main issues in the study on flight vehicle control nowadays is actuator failure [1,2]. A thorough research has recently been conducted to describe every possible issue that could arise with a flight vehicle system [3]. The primary flight control systems have adopted hybrid actuation systems to increase reliability and safety. One such example is the Airbus A320, which uses a hybrid actuation system to power the aileron, rudder, and elevator [4]. The actuators are an important component of the flight control system due to their responsibility for controlling the motion of the aircraft's control surface [5]. For a long time, hydraulic power was the only source of power for actuators to drive the aircraft's control surface. Later, safety and reliability became the most important topics in the flight control system. With the advancement of the aircraft industry, a similar redundant actuation configuration was introduced to meet the requirements of safety and reliability. Later, it

was found that safety risk is still a problem when common-mode/common-cause errors occur in similar redundant actuation systems. It put limitations on further advancement in the safety and reliability of similar redundant actuation systems [6,7]. Further progress in research on redundant actuation systems gave us the idea to introduce an electro-mechanical actuator into redundant actuation systems along with a hydraulic actuator so that the aircraft industry can overcome the problem of common-mode and common-cause error and enhance the reliability and safety of redundant actuation systems [8,9].

Finally, the progress in research helped us to develop a heterogeneous drive actuation system (hybrid actuation system) composed of electro-hydraulic servo actuators (SHA) and electro-mechanical actuators (EMA), which improves the safety and reliability of the actuation part of aircraft [10]. The research on more electric aircraft (MEA) has enabled the ability to increase reliability by introducing electric motors, electrical distribution systems, generator drives, actuators, and power electronics [11,12]. A combination of SHA and EMA helped to develop an SHA/EMA hybrid actuation system that fulfils the demand for high safety and reliability. Furthermore, it reduces common-mode and common-cause errors, ultimately resulting in an increase in the robustness and efficiency of the aircraft's actuation system [13].

The past research helped us to develop an SHA/EMA hybrid actuation system (HAS), but there are still some problems associated with the SHA/EMA hybrid actuation system, and these problems must be addressed. The SHA and EMA both have different dynamics. They produce different displacement output under the same pilot command input signal, and their output force is also different under the same input signal. This is happening due to the different working principles of SHA and EMA [14]. There will be an intercoupling effect (between EMA and SHA) when both actuators are connected to the aircraft control surface via rigid coupling. Force fighting occurs when the control surface of an aircraft is pushed together by both actuators. The difference in output force of two dissimilar redundant actuators is referred to as "force fighting". Force fighting affects the tracking efficiency of the aircraft control surface, and can result in damage to the control surface [7]. So, the aviation industry needs to design a controller that can solve the problem of force fighting and easily synchronize the motion of two actuators. Salman did some efforts to solve this problem of force by using different types of control techniques [15–19]. It was found that synchronization is an important task in motion control to reduce force fighting [20,21]. Later, the aviation industry started to focus on the design of synchronization controllers. An average actuator force difference and real actuator force were imported into the integrator to eliminate force fighting by producing a position demand offset in order to achieve synchronous output force from two unlike actuators [22]. The studies have also demonstrated the design of controllers that encounter the static force fighting for an HAS (hybrid actuation system) composed of an EMA and SHA [14,23]. Moreover, for further improvement in tracking control precision and accuracy, uncertainties, external disturbances, and nonlinear dynamics, along with the coupling effect between EMA and EHSA, must be considered while designing the controller. The motion-state synchronization method is an efficient way to deal with the problem of forces fighting between the two different actuators. Motion-state synchronization can be used to keep such actuators' motion states, such as displacement, velocity, acceleration, jerk, etc., stable [7]. Rehman has focused the motion synchronization for electro-hydrostatic and servo-hydraulic hybrid actuation systems using different types of control techniques [24–28]. Wang made some efforts to propose sensor-less control for motion synchronization of the hybrid actuation system [29–31]. Progress in the research of hybrid actuation systems helped Cochoy et al. to develop a force equalization controller by employing state signals of displacement, velocity, and force [8], according to the ideal hypothesis which states that all contributed signals are important to develop a controller. Getting these state variables allows the created hybrid actuation system to predict the system movement. However, it is tough to acquire the entire state signals of a physical actuation system in an airplane. In order to deal with this matter, an HAS (hybrid actuation system) test bench was developed to achieve all-state signals

by introducing several sensors [10]. However, this method would significantly raise the weight and cost of the actuators which would limit their application. In the current research, a nested-loop intelligent control technique is presented that is comprised of trajectory, force controller, and position controller for each actuator.

2. Problem Description

The SHA, EMA, and control surface are the key components of a hybrid actuation system (HAS), and are depicted in Figure 1. An electrically-driven actuator that controls the flow of hydraulic fluid to an actuator is known as a servo-hydraulic actuator (SHA). Powerful hydraulic cylinders are frequently controlled by servo valves using a very small electrical signal. Servo valves have good post-movement damping qualities and can offer fine control of position, velocity, pressure, and force. An electro-mechanical actuator (EMA) is a tool that uses an electric motor to transform electricity into mechanical force. Electric motors turn a spindle in a rotating motion by using an electric current. Through the employment of gears, this rotating motion is transformed into linear motion. u_{sv} and u_m are used as an input control signal for SHA and EMA, respectively. The EMA and SHA are rigidly coupled to the aircraft control surface. SHA has a servo valve as an actuating element, while EMA has an electric motor. When two actuators push the control surface of an aircraft together, they produce force fighting. Force fighting is the difference between the output forces of two actuators. Force fighting can be eliminated when two actuators contribute equally to driving the control surface. The SHA is faster than the EMA; that is the reason for force fighting. EMA is slower because the response time of the motor is large as compared to the servo valve. Force fighting can be removed by synchronizing the motion of two actuators so they contribute equally to drive the control surface of the aircraft. Mathematically it is given by:

$$\text{Force Fighting} \;=\; F_{fight} \;= F_s - F_m \tag{1}$$

$$F_{fight} \;= F_s - F_m = k_s(x_s - x_c) - k_m(x_m - x_c) \tag{2}$$

$$F_{fight} \;= F_s - F_m = k(x_s - x_m) \qquad \therefore k_m = k_s = k \tag{3}$$

where F_s is force delivered by SHA, F_m is force delivered by EMA, x_s is displacement given by SHA, x_m is displacement given by EMA, and x_c is linear motion of aircraft's control surface. The analysis of Equation (3) shows that a hybrid actuation system will have no force fighting when both actuators have the same displacement, provided the transmission stiffness is the same for both actuators.

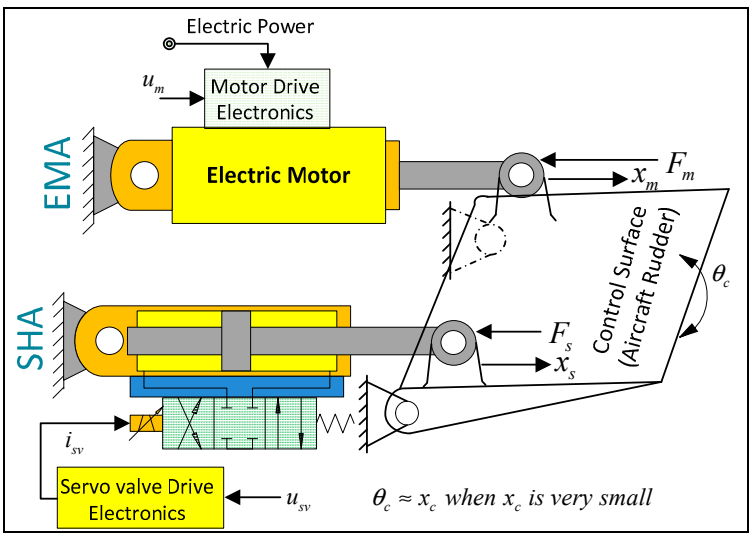

Figure 1. Configuration for SHA/EMA HAS.

3. Mathematical Model of Hybrid Actuation System (HAS)

The hybrid actuation system is composed of the control surface, electro-mechanical actuator, and servo-hydraulic actuator, which will be modeled one by one.

3.1. Modelling of Aircraft's Control Surface

According to the law of motion, the dynamics involved in the motion of the control surface of the aircraft are given by:

$$(F_s + F_m)r_c = j_c\ddot{\theta}_c + F_{air}r_c \tag{4}$$

$$F_s = k_s(x_s - x_c) \tag{5}$$

$$F_m = k_m(x_m - x_c) \tag{6}$$

where j_c is inertial moment and r_c is the radial displacement which appears during angular motion θ_c. The k_s is the stiffness coefficient for SHA and k_m is the stiffness coefficient for EMA. It is found that the magnitude of angular displacement is very small. In such scenarios, θ_c and x_c (linear movement of aircraft control surface) can be taken to be linear [32], and given by the relationship:

$$x_c = \theta_c r_c \tag{7}$$

3.2. Mathematical Model of SHA

The servo-valve actuator consists of the servo valve, hydraulic cylinder, and additional accessories. The servo valve is a very effective element for fluid transmission control and widely used in many applications for controlling the transmission of fluid where the end result is motion control through fluid power [33,34]. According to previous studies, the dynamics of a servo valve and a hydraulic cylinder is given by [14]:

$$x_{sv} = k_{sv}u_{sv} \tag{8}$$

$$Q_{sv} = k_{sq}x_{sv} - k_{sc}p_f \tag{9}$$

where x_{sv} is displacement of the spool of the servo valve, u_{sv} is an input signal to the coil of the servo valve and k_{sq} is flow/opening gain, and k_{sc} is flow/pressure gain.

The force dynamics and the flow dynamics of a servo-hydraulic actuator is given by [14,35]:

$$\begin{aligned} Q_{sv} &= A_j\dot{x}_s + \tfrac{v_j}{4E_j}\dot{p}_f + k_{ac}p_f \\ F_j &= m_j\ddot{x}_s + B_j\dot{x}_s + F_s \end{aligned} \tag{10}$$

where A_j is piston effective area, p_f is load pressure, v_j is piston effective volume, k_{ac} is the leakage coefficient, E_j is the oil bulk modulus, $F_j = A_j p_f$ is the force provided by the jack, m_j is the piston mass, and B_j is damping coefficient.

Define $x_1 = [x_{11}, x_{12}, x_{13}]^T = [x_s, \dot{x}_s, \ddot{x}_s]^T$ as the state vector of SHA system and let suppose $u_1 = u_{sv}$. The state space form of SHA can be given as:

$$\Omega_{SHA} = \begin{cases} \dot{x}_{11} = x_{12} \\ \dot{x}_{12} = x_{13} \\ \dot{x}_{13} = f_1(x_1) + g_1 + \sigma_1 u_1 \end{cases} \tag{11}$$

where:

$$f_1(x_1) = -\frac{4E_j k_{hs}(k_s + k_{ac})}{m_j v_j}x_{11} - \frac{4E_j A_j^2 + 4E_j B_j(k_s + k_{ac}) + v_j}{m_j v_j}x_{12} - \frac{4E_j m_j(k_s + k_{ac}) + B_j v_j}{m_j v_j}x_{13}$$

$$g_1 = \frac{4E_j k_{hs}\left(k_{sq} + k_{ac}\right)}{m_j v_j} x_c - \frac{k_{hs}}{m_j}\dot{x}_c$$

$$\sigma_1 = \frac{4A_j E_j k_{sq} k_{sv}}{m_j v_j}$$

3.3. Mathematical Model of EMA

The electrical dynamics of an electric motor which is present in an electro-mechanical actuator, is given by [10,36]:

$$u_m = k_m \omega_m + L_m \frac{di_m}{dt} + R_m i_m \tag{12}$$

$$T_m = k_{bm} i_m \tag{13}$$

R_m, i_m, and L_m are resistance, current, and inductance of armature, respectively. k_{bm} is back-emf constant, ω_m is the angular velocity, and T_m is electro-magnetic torque. The torque provided by the motor is converted into load torque and inertial dynamics and overcomes the damping dynamics.

$$T_m - T_L = j_m \frac{d\omega_m}{dt} + B_m \omega_m \tag{14}$$

where j_m is total inertia, B_m is damping constant, and T_L is load torque. The transition relationship between rotational and translational parts is given by:

$$\begin{cases} \dot{x}_m = \frac{1}{\eta_m k_{gm}} \omega_m \\ T_L = \frac{1}{\eta_m k_{gm}} F_m \end{cases} \tag{15}$$

where η_m is transmission efficiency and k_{gm} is transmission coefficient.

Let suppose state vectors for an electro-mechanical actuator are $x_2 = [x_{21}, x_{22}, x_{23}]^T = \left[x_m, \dot{x}_m, \ddot{x}_m\right]^T$ and control input is $u_2 = u_m$. The state space for EMA is given by:

$$\Omega_{EMA} = \begin{cases} \dot{x}_{21} = x_{22} \\ \dot{x}_{22} = x_{23} \\ \dot{x}_{23} = f_2(x_2) + g_2 + \sigma_2 u_2 \end{cases} \tag{16}$$

where:

$$f_2(x_2) = -\frac{R_m k_{ms}}{L_m j_m k_{gm}^2 \eta_m^2} x_{21} - \frac{k_{bm} k_m k_{gm}^2 \eta_m^2 + L_m k_{ms} + R_m B_m k_{gm}^2 \eta_m^2}{L_m j_m k_{gm}^2 \eta_m^2} x_{22} - \frac{B_m L_m + j_m R_m}{j_m L_m} x_{23}$$

$$g_2 = \frac{R_m k_{ms}}{L_m j_m k_{gm}^2 \eta_m^2} x_c + \frac{k_{ms}}{j_m k_{gm}^2 \eta_m^2} \dot{x}_c$$

$$\sigma_2 = \frac{k_{bm}}{L_m j_m k_{gm} \eta_m}$$

4. Nested-Loop Intelligent Control Strategy

It is very difficult to synchronize an SHA/EMA system with just one controller due to inconsistent dynamics between SHA and EMA. So, a nested-loop intelligent control strategy is proposed for SHA/EMA systems. This proposed technique is made up of a trajectory generator, force controller, and position controller as shown in Figure 2. Where X_{tr} is the reference position, $\dot{X}_{\text{tr}}$ is the reference velocity, and $\ddot{X}_{\text{tr}}$ is the reference acceleration signal. u_1 and u_2 are position controller's output of the SHA and the EMA, respectively. u_{11} and u_{21} are the outputs of the force controller for the SHA and the EMA, respectively.

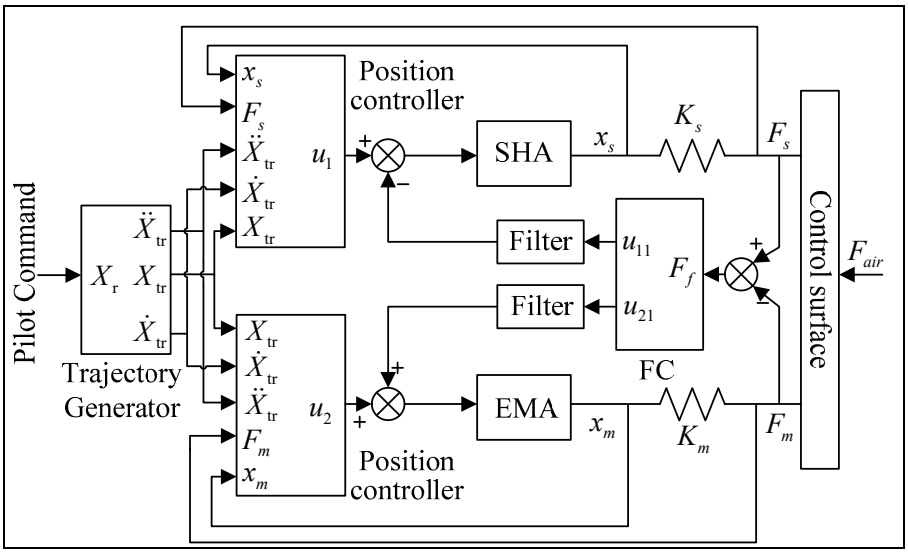

Figure 2. Structure of hybrid SHA/EMA system.

4.1. Trajectory Generator

The trajectory-based systems perform well in the desired motion tracking application; that is why a trajectory is designed. The desired motion is achieved by a trajectory generator which generates position (x_{tr}), velocity ($\dot{x}_{tr}$), and acceleration ($\ddot{x}_{tr}$) signals. The desired trajectory designed by [24,37,38] is used. It is the second order-transfer function which is given by:

$$x_{tr} = \frac{\omega_{tr}^2}{s^2 + 2\xi_{tr}\omega_{tr}s + \omega_{tr}^2} x_r \tag{17}$$

where

ω_{tr} = Reference natural frequency
ξ_{tr} = Reference damping factor
x_r = Reference input signal

The ideal trajectory is depicted in the left portion of Figure 3, while the realistic and practical trajectory is depicted in the right portion. There are two saturation thresholds: one for acceleration and one for velocity. The maximum speed is ±0.12 m/s, while the maximum acceleration is ±2 m/s. According to the dynamics of EHA, two trajectory parameters are set.

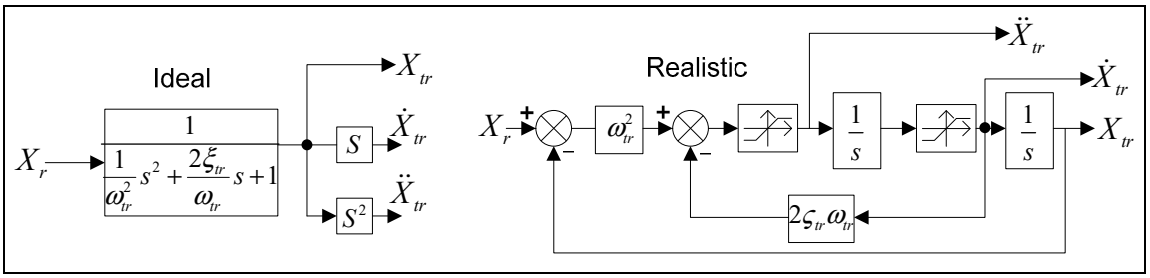

Figure 3. Schematic of second order trajectory.

4.2. Position Controller

The position controller is made up of two parts: an intelligent position controller and feed-forward control. Both work together to improve the position tracking performance of the SHA/EMA system. The feed-forward control responds to disturbances in a predefined manner. It is designed to predict the behavior of the system. It responds before an error occurs. In this way, it helps to control sluggish dynamics and delay in the SHA/EMA system. The feed-forward control is designed for both

SHA and EMA to follow a desired trajectory so that the system can be synchronized. Feed-forward controllers for SHA and EMA are given by:

$$u_{SHA} = \frac{1}{k_{sv}k_{sq}}\left[A_j\dot{x}_{tr} + \frac{1}{A_j}\left(\frac{v_j}{4E_j} + k_{ce}\right)\left(m_j\ddot{x}_{tr} + B_j\dot{x}_{tr} + F_s\right)\right] \tag{18}$$

$$u_{EMA} = k_m k_{gm}\eta_m\dot{x}_{tr} + \frac{(L_m s + R_m)}{k_{bm}}\left[(j_m s + B_m)k_{gm}\eta_m\dot{x}_{tr} + \frac{1}{k_{gm}\eta_m}F_m\right] \tag{19}$$

The use of fuzzy logic to control position is gaining popularity in recent days [39–41]. That is why a fuzzy logic-based PID controller is used for the position. The performance is enhanced due to the variable gain of tuning parameters that vary with the help of membership functions. The advantage is overcoming time delays and dealing with models that are not precise and accurate. The intelligent position tracking controller consists of two parts, such as a PID controller and a fuzzy logic controller. The PID controller is given by (20) while a proper range of each tuning parameter is found by using a mechanism which is given in (21).

$$u_n = \left(K'_pG_1 + G_2\right)e(t) + \left(K'_iC_1 + C_2\right)\int_0^t e(t) + \left(K'_dD_1 + D_2\right)\dot{e}(t) \quad \therefore n \in \{SHA, EMA\} \tag{20}$$

$$K_z = (K_{\mathrm{zmax}} - K_{\mathrm{zmin}})K'_z + K_{\mathrm{zmin}} \qquad \therefore z \in \{P, I, D\} \tag{21}$$

where $C_1 = K_{imax} - K_{imin}$, $C_2 = K_{imin}$, $G_1 = K_{pmax} - K_{pmin}$, $G_2 = K_{pmin}$, $D_1 = K_{dmax} - K_{dmin}$, $D_2 = K_{dmin}$, K'_{p}, K'_{i}, and K'_d are the tuning parameters which are tuned by a fuzzy logic controller. Subscript z represents a type of tuning parameter; it may be derivative, integral, or proportional.

The fuzzy logic produces the desired value of tuning parameters according to input of error e_p and change in error ($\dot{e}_p$). The position error (e_p) and change in position ($\dot{e}_p$) is fed into the fuzzy position controller, and the control inputs to the actuator can be determined from fuzzy rules presented in Table 1. Fuzzy input sets are mapped to a set of linguistic labels: negative big (NB), negative small (NS), zero (ZE), positive small (PS), and positive big (PB), over the ranges of the input variables. The output fuzzy sets correspond to the labels: small (S), medium small (MS), big (B), and medium big (MB) over the two output variable ranges. Table 1's fuzzy rules are separated into four sections. Rising times are dominated by region 1 (the red region). Region 2 (the yellow region) predominates at its greatest overshoot time. The dominant region in the convergence stage is region 3 (light black). Region 4 (the white region) rules at steady state. There are four basic building blocks in the fuzzy logic controller. ① Rule base ② Inference mechanisms ③ Fuzzification ④ Defuzzification. ① Rule base: keeps information in the form of rules and a set of rules for the proposed system is given in Table 1. Each rule shows the states of membership functions. The membership functions are given in Table 2 and graphically presented in Figure 4.

Table 1. Fuzzy rules for the fuzzy position controller.

Change of Error ($\dot{e}_p$)	**Error e_p**					**Region 1**
	NB	**NS**	**ZE**	**PS**	**PB**	
NB	S	S	MS	MS	M	Region 2
NS	S	MS	MS	M	MB	
ZE	MS	MS	M	MB	MB	Region 3
PS	MS	M	MB	MB	B	
PB	M	MB	MB	B	B	Region 4

Note: NB: Negative big; NS: Negative small; PB: Positive big; PS: Positive small; ZE: Zero; S: Small; MS: Medium small; M: Medium; MB: Medium big; B: Big.

Table 2. The fuzzy position controller's membership functions.

Parameters in Membership Function	Membership Function														
	e_p					$\dot{e}_p$					K_p', K_i', K_d'				
	NB	**NS**	**ZE**	**PS**	**PB**	**NB**	**NS**	**ZE**	**PS**	**PB**	**S**	**MS**	**M**	**MB**	**B**
a_r	−15	−10	−5	0	5	−75	−50	−25	0	25	0.1	0.15	0.30	0.5	0.7
b_r	−10	−5	0	5	10	−50	−25	0	25	50	0.15	0.3	0.5	0.7	1
c_r	−5	0	5	10	15	−25	0	25	50	75	0.3	0.5	0.7	1	1.15

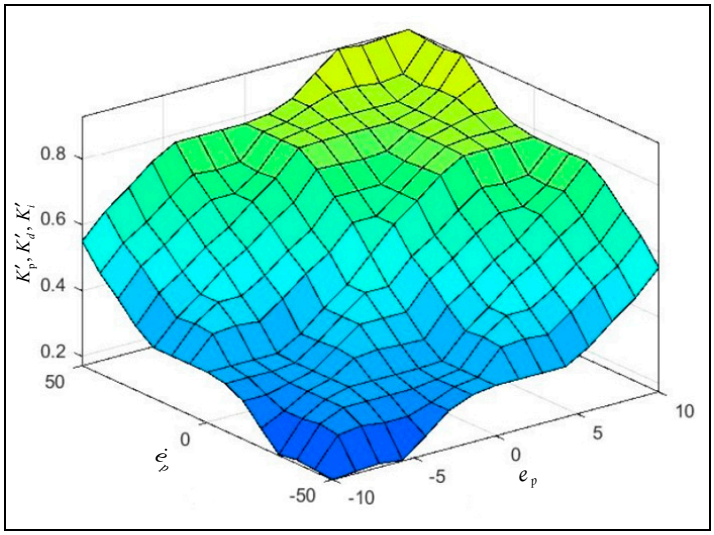

Figure 4. Graphical presentation for membership function of fuzzy position controller.

The fuzzy rules are kept the same to get different tuning parameters while member functions change. ② Fuzzy inference mechanisms: interfaces with the rule base and makes a decision to choose a proper value of the tuning parameter. ③ The fuzzification: Convert input into such forms that are interpretable and can be compared to the rules. ④ Defuzzification: it produces tuning parameter values based on the judgments of fuzzy interference processes.

The triangular member function is used and is defined as:

$$\mu_r = \begin{cases} 0 & x \le a_r \\ (x - a_r)/(b_r - a_r) & a_r < x < b_r \\ (c_r - x)/(c_r - b_r) & b_r < x < c_r \\ 0 & c_r \le x \end{cases} \tag{22}$$

where r belongs to the following set [NB, NS, ZE, PS, PB, S, MS, M, MB, B].

4.3. Force Controller

The position controller tries to achieve motion synchronization between SHA and EMA by improving position tracking performance, while the force controller (FC) tries to achieve motion synchronization for SHA/EMA by improving force tracking performance. Force controller is a fuzzy based PID controller. Its hybrid structure is shown in Figure 5.

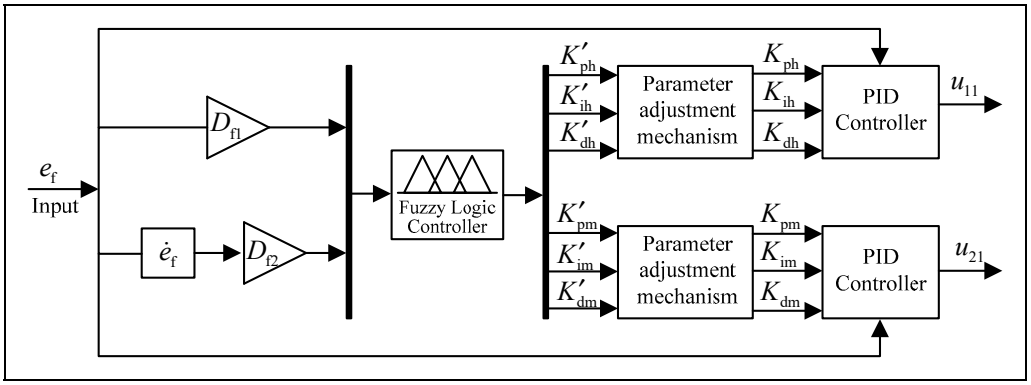

Figure 5. Hybrid Structure for fuzzy based PID control.

The D_{f1} and D_{f2} are input gains that convert input error into such a form which can conveniently interface with a fuzzy logic controller. The $\left[K'_{ph}, K'_{ih}, K'_{dh}\right]$ and $\left[K'_{pm}, K'_{im}, K'_{dm}\right]$ are tuning gains by a fuzzy logic controller for SHA and EMA, respectively. The $\left[K_{ph}, K_{ih}, K_{dh}\right]$ and $\left[K_{pm}, K_{im}, K_{dm}\right]$ are tuning parameters of PID controllers for SHA and EMA, respectively. u_{11} and u_{21} are the output of force controller, which are determined on the basis of fuzzy rules and membership function. The fuzzy rules are given in Table 3 and the membership functions are given in Table 4. The error (e_f) and change in error ($\dot{e}_f$) are fed into the fuzzy force controller, and the control inputs to the actuator can be determined from fuzzy rules presented in the Table 3. Table 3's fuzzy rules are separated into four sections. Rising times are dominated by region 1 (the red region). Region 2 (the yellow region) predominates at its greatest overshoot time. The dominant region in the convergence stage is region 3 (light black). Region 4 (the white region) rules at steady state.

Table 3. Fuzzy rules for the Force controller.

Change of Error $\dot{e}_f$	**Error** e_f					
	NB	**NS**	**ZE**	**PS**	**PB**	**Region 1**
NB	M	MB	B	B	B	Region 2
NS	MS	M	MB	MB	B	
ZE	S	MS	M	MB	B	Region 3
PS	S	MS	MS	M	MB	
PB	S	S	S	MS	M	Region 4

Table 4. Membership functions for the force controller.

Parameters in Membership Function	**Membership Function**																			
	e_f					$\dot{e}_f$					$K'_{ph}, K'_{ih}, K'_{dh}, K'_{im}, K'_{dm}$					K'_{pm}				
	NB	**NS**	**ZE**	**PS**	**PB**	**NB**	**NS**	**ZE**	**PS**	**PB**	**S**	**MS**	**M**	**MB**	**B**	**S**	**MS**	**M**	**MB**	**B**
a_r	−100	−10	−5	0	5	−100	−8	−4	0	4	0.1	0.15	0.3	0.5	0.7	0.87	0.90	0.92	0.95	0.97
b_r	−10	−5	0	5	10	−8	−4	0	4	8	0.15	0.3	0.5	0.7	1	0.90	0.92	0.95	0.97	1
c_r	−5	0	5	10	100	−4	0	4	8	100	0.3	0.5	0.7	1	1.15	0.92	0.95	0.97	1	1.15

5. Result and Discussion

To evaluate the performance of the suggested intelligent control method, a mathematical model for the hybrid actuation system of the SHA/EMA is developed in Matlab/Simulink. The simulations are performed by using simulation parameters which are given in Table 5. In order to compare results

between classical PID control (tuned via particle swarm optimization) and the proposed nested-loop intelligent control strategy, the following notation will be used: C_{PID} and $C_{Intelligent}$ for PID and the proposed nested-loop intelligent control strategy, respectively.

Table 5. Parameters for SHA/EMA actuation systems.

SHA/EMA Parts	Parameters			Values	Units
Servo-hydraulic Actuator (SHA)	Gain Coefficient k_{sv}			3.04×10^{-4}	m/A
	Flow /opening gain k_{sq}			2.7	m^2/s
	Flow / pressure gain k_{sc}			1.75×10^{-11}	$(m^3/s)Pa$
	Area of Piston A_j			1.1×10^{-3}	m^2
	Cylinder chamber volume v_j			1.1×10^{-4}	m^3
	Mass of piston including chamber m_j			25	Kg
	Damping constant B_j			1×10^4	N·s/m
	Bulk modulus constant E_j			8×10^8	Pa
	Coefficient of Leakage k_{ac}			1×10^{-11}	$(m^3/s)Pa$
Electro-mechanical Actuator (EMA)	Bake emf constant k_m			0.161	V/(rad/s)
	Armature Inductance L_m			4.13×10^{-3}	H
	Armature resistance R_m			0.54	Ω
	Electro-magnetic coefficient k_{bm}			0.64	Nm/A
	Total inertia of rotating parts j_m			1.136×10^{-3}	Kg·m^2
	Damping coefficient B_m			4×10^{-3}	Nm·s/rad
	Transmission coefficient k_{gm}			1.256×10^3	rad/m
	Transmission efficiency η_m			0.9	
Control Surface	Connection stiffness	SHA	k_s	1×10^8	N/m
		EMA	k_m		
	Radial distance for control surface r_{cs}			0.1	m
	Moment of inertia for control surface j_{cs}			6.0	Kg·m^2

5.1. Results with Step Signal as Input Command

The step input command is given to a hybrid actuation system of SHA/EMA with an amplitude of 30 (mrad). It is found that displacement of the control surface of SHA/EMA is controlled by intelligent control strategy and follows the input signal better than the displacement of the control surface of SHA/EMA controlled by the PID controller, as shown in Figure 6. To check the disturbance rejection performance of the proposed intelligent control strategy against PID control for SHA/EMA, a jerk load is applied when time is 2.5 s. It is found that the maximum deviation for intelligent control strategy is 1 (mrad) using reference input signal while for PID control is 3 (mrad) using reference input signal in region 1.

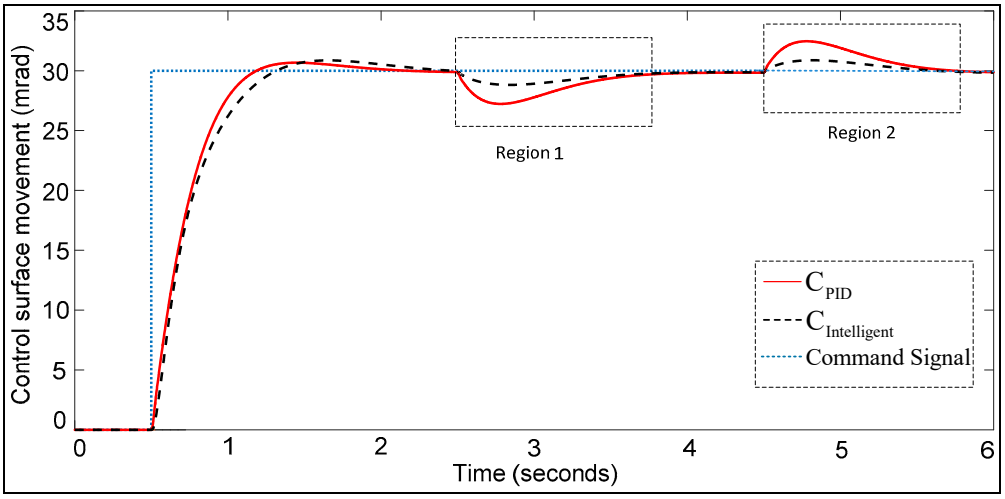

Figure 6. Tracking response against step input command.

In terms of disturbance rejection, the intelligent control technique performs better than PID control. Following the completion of the jerk load, region 2 illustrates how the intelligent control system swiftly locates an equilibrium position. Additionally, as demonstrated in Figure 7, the tracking error for the suggested intelligent control technique is lower than that of PID control.

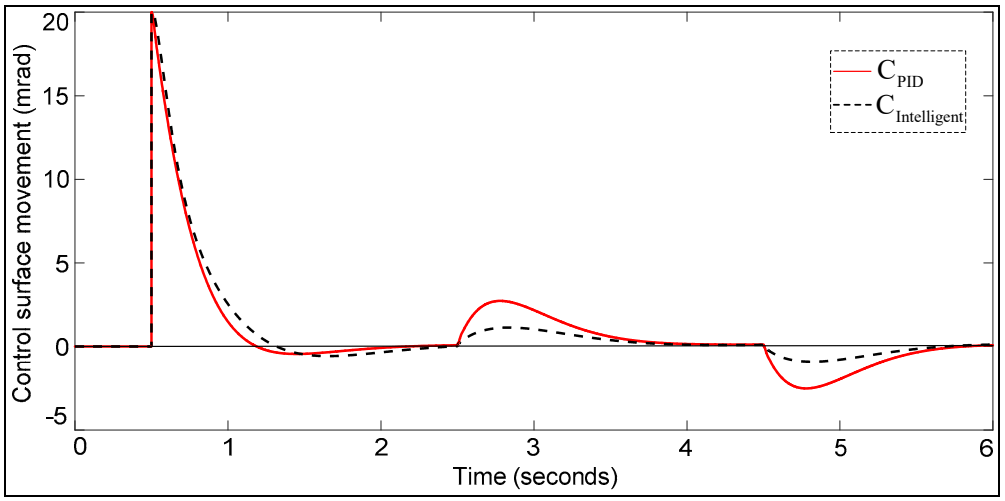

Figure 7. Tracking error by step input command.

The force fighting is basically the force difference between two different actuators such as SHA and EMA. It is due to different dynamic characters of SHA and EMA. In Figure 8, region 1 represents initial force fighting. An initial force fighting for PID control is found to be 16.3 KN, while for an intelligent control strategy, it is 3.7 KN. Similarly, when jerk load acts on control surface, then force fighting for PID control is 9.7 KN while for intelligent control it is 8KN, as shown in region 2 of Figure 8. A similar attitude is shown in region 3 of Figure 8. The result shows that the SHA/EMA hybrid actuation system has less force fighting under proposed intelligent control strategy as compared to PID control strategy.

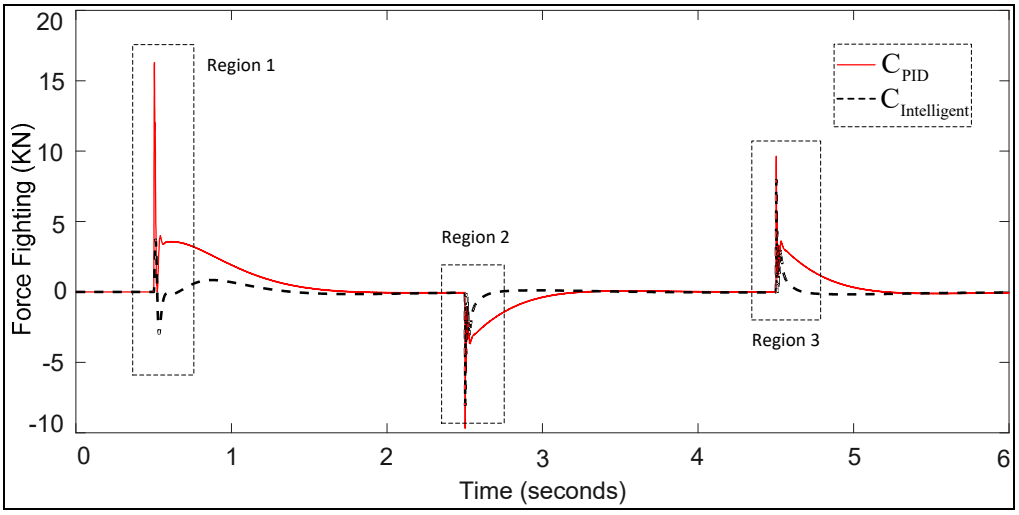

Figure 8. Force fighting by step input command.

5.2. Results with Dynamic Signal as Input Command

The dynamic signal is given as an input command to a hybrid actuation system of SHA/EMA. It is found that the displacement of the control surface of SHA/EMA controlled by the intelligent control strategy follows the input command signal better than the displacement of the control surface of SHA/EMA controlled by the PID controller, as shown in Figure 9.

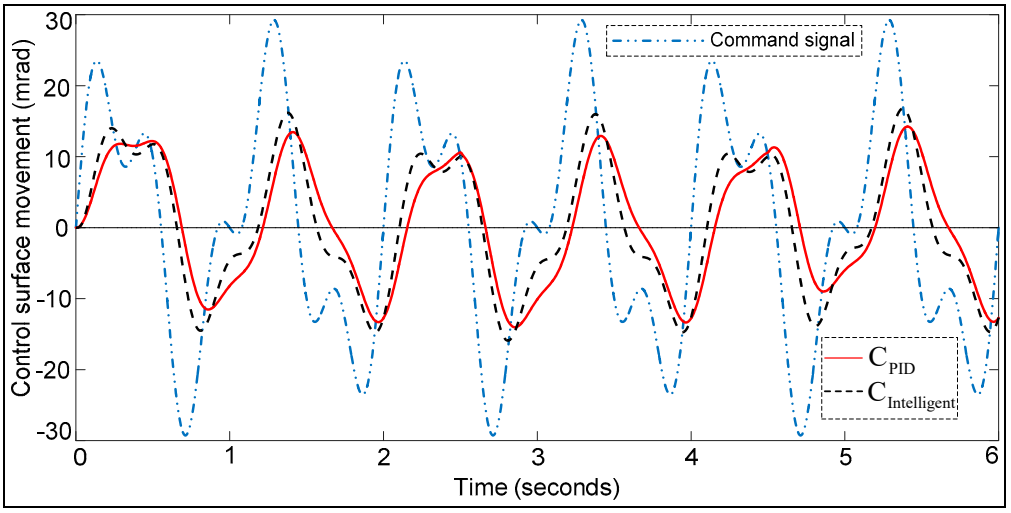

Figure 9. Tracking response by dynamic signal as input command.

To check the disturbance rejection performance of the proposed intelligent control strategy against PID control for SHA/EMA, a jerk load is applied when the time is 2.5 s. As shown in Figure 9, the SHA/EMA actuation system under intelligent control strategy always follows the reference command signal quickly, even after external force is applied. In order to carry out a better analysis of tracking errors, two regions are taken, such as region 1 and region 2, as shown in Figure 10. Region 1 depicts the tracking error prior to the application of external load force, whereas region 2 depicts the tracking error following the application of external load force. As illustrated in Figure 10, both regions show that the tracking error produced by the SHA/EMA actuation system controlled by intelligent control is always less than the tracking error produced by the SHA/EMA control system controlled by PID.

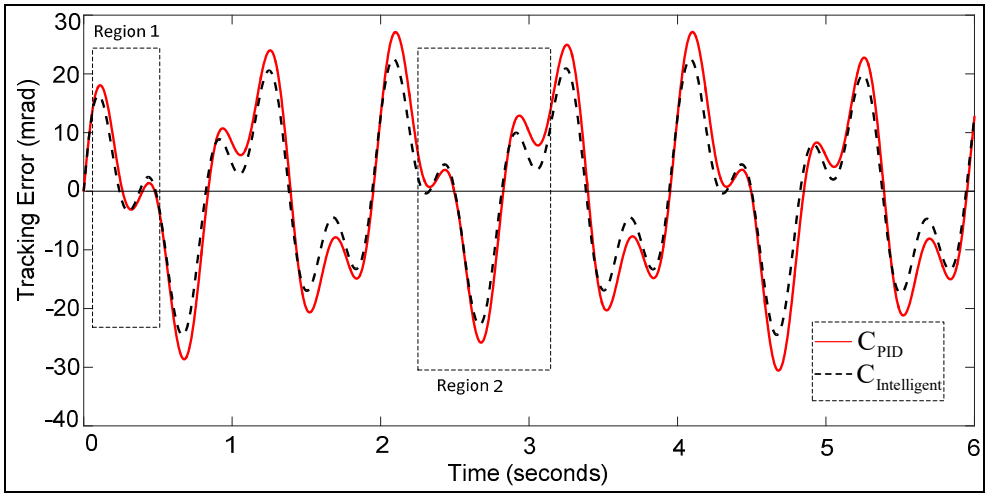

Figure 10. Tracking error by dynamic signal as input command.

The force fighting is basically the force difference between two different actuators such as SHA and EMA. It is due to the different dynamic characters of SHA and EMA. In Figure 11, the black dotted line shows the force fighting by the SHA/EMA system which is controlled by intelligent control strategy while the continuous red solid line shows the force fighting of the SHA/EMA system which is controlled by PID. Figure 11 clearly shows that force fighting due to an intelligent control system is less as compared to a PID control system.

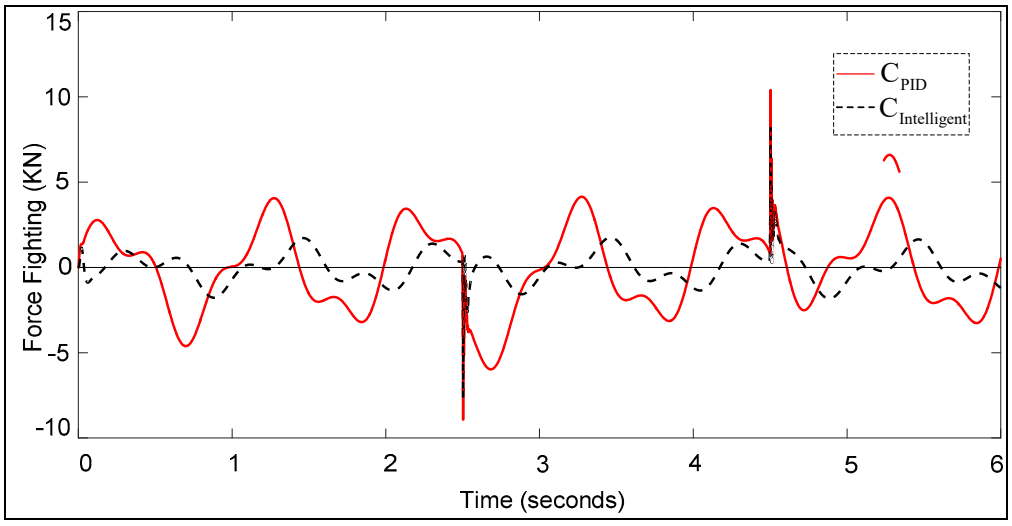

Figure 11. Force fighting by dynamic signal as input command.

6. Conclusions

This paper focuses on intelligent control system design for hybrid actuation systems composed of servo-hydraulic actuators and electro-mechanical actuators. A trajectory, force controller, and position controller are also components of an intelligent control strategy of the nested loop kind. A feed-forward controller and a PID controller with fuzzy logic are also parts of the position controller. The outcomes have demonstrated that the feed-forward controller and position controller work in tandem to synchronize the SHA and EMA and enable the control surface to move along the appropriate trajectory with the least amount of force fighting. The outcome demonstrates that the force controller further enhances SHA and EMA's synchronization so that both can equally drive the external aircraft control surface. The simulations have been done in Matlab/Simulink under different conditions of external air load and pilot command signal. The results show that the SHA/EMA system under the proposed nested-loop control strategy performs well as compared to the PID control strategy.

Author Contributions: Software, W.U.R.; Validation, W.U.R.; Writing—original draft, W.U.R.; Writing—review & editing, W.U.R.; Visualization, Z.H. and M.Y.G.; Supervision, X.W. All authors have read and agreed to the published version of the manuscript.

Funding: This research received no external funding.

Conflicts of Interest: The authors declare that they have no conflict of interest.

References

1. Benchaita, H.; Ladaci, S. Fractional adaptive SMC fault tolerant control against actuator failures for wing rock supervision. *Aerosp. Sci. Technol.* **2021**, *114*, 106745. [CrossRef]
2. Ynineb, A.R.; Ladaci, S. MRAC adaptive control design for an F15 aircraft pitch angular motion using Dynamics Inversion and fractional-order filtering. *Int. J. Robot. Control Syst.* **2022**, *2*, 240–252. [CrossRef]
3. Karpenko, M. Landing gear failures connected with high-pressure hoses and analysis of trends in aircraft technical problems. *Aviation* **2022**, *26*, 145–152. [CrossRef]
4. Haitao, Q.; Yongling, F.; Xiaoye, Q.; Yan, L. Architecture optimization of more electric aircraft actuation system. *Chin. J. Aeronaut.* **2011**, *24*, 506–513.
5. Goupil, P. AIRBUS state of the art and practices on FDI and FTC in flight control system. *Control Eng. Pract.* **2011**, *19*, 524–539. [CrossRef]
6. Van Den Bossche, D. The A380 flight control electrohydrostatic actuators, achievements and lessons learnt. In Proceedings of the 25th International Congress of the Aeronautical Sciences, Hamburg, Germany, 3–8 September 2006; pp. 1–8.
7. Shi, C.; Wang, X.; Wang, S.; Wang, J.; Tomovic, M.M. Adaptive decoupling synchronous control of dissimilar redundant actuation system for large civil aircraft. *Aerosp. Sci. Technol.* **2015**, *47*, 114–124. [CrossRef]
8. Cochoy, O.; Hanke, S.; Carl, U.B. Concepts for position and load control for hybrid actuation in primary flight controls. *Aerosp. Sci. Technol.* **2007**, *11*, 194–201. [CrossRef]
9. Fu, J.; Maré, J.-C.; Fu, Y. Modelling and simulation of flight control electromechanical actuators with special focus on model architecting, multidisciplinary effects and power flows. *Chin. J. Aeronaut.* **2017**, *30*, 47–65. [CrossRef]
10. Cochoy, O.; Carl, U.B.; Thielecke, F. Integration and control of electromechanical and electrohydraulic actuators in a hybrid primary flight control architecture. In Proceedings of the International Conference on Recent Advances in Aerospace Actuation Systems and Components, Insa Toulouse, France, 13–15 June 2007; pp. 1–8.
11. Emadi, K.; Ehsani, M. Aircraft power systems: Technology, state of the art, and future trends. *IEEE Aerosp. Electron. Syst. Mag.* **2000**, *15*, 28–32. [CrossRef]
12. Naayagi, R. A review of more electric aircraft technology. In Proceedings of the 2013 International Conference on Energy Efficient Technologies for Sustainability, Nagercoil, India, 10–12 April 2013; pp. 750–753.
13. Rosero, J.; Ortega, J.; Aldabas, E.; Romeral, L. Moving towards a more electric aircraft. *IEEE Aerosp. Electron. Syst. Mag.* **2007**, *22*, 3–9. [CrossRef]
14. Wang, L.; Mare, J.-C. A force equalization controller for active/active redundant actuation system involving servo-hydraulic and electro-mechanical technologies. *Proc. Inst. Mech. Eng. Part G J. Aerosp. Eng.* **2014**, *228*, 1768–1787. [CrossRef]
15. Salman, I.; Lin, Y.; Hamayun, M.T. Fractional order modeling and control of dissimilar redundant actuating system used in large passenger aircraft. *Chin. J. Aeronaut.* **2018**, *31*, 1141–1152.
16. Ijaz, S.; Yan, L.; Hamayun, M.T.; Shi, C. Active fault tolerant control scheme for aircraft with dissimilar redundant actuation system subject to hydraulic failure. *J. Frankl. Inst.* **2019**, *356*, 1302–1332. [CrossRef]
17. Ijaz, S.; Hamayun, M.T.; Yan, L.; Ijaz, H.; Shi, C. Adaptive fault tolerant control of dissimilar redundant actuation system of civil aircraft based on integral sliding mode control strategy. *Trans. Inst. Meas. Control* **2019**, *41*, 3756–3768. [CrossRef]
18. Ijaz, S.; Hamayun, M.T.; Anwaar, H.; Yan, L.; Li, M.K. LPV modeling and tracking control of dissimilar redundant actuation system for civil aircraft. *Int. J. Control Autom. Syst.* **2019**, *17*, 705–715. [CrossRef]
19. Ijaz, S.; Yan, L.; Hamayun, M.T.; Baig, W.M.; Shi, C. An adaptive LPV integral sliding mode FTC of dissimilar redundant actuation system for civil aircraft. *IEEE Access* **2018**, *6*, 65960–65973. [CrossRef]
20. Cieplok, G.; Wójcik, K. Conditions for self-synchronization of inertial vibrators of vibratory conveyors in general motion. *J. Theor. Appl. Mech.* **2020**, *58*, 513–524. [CrossRef]
21. Fang, P.; Zou, M.; Peng, H.; Du, M.; Hu, G.; Hou, Y. Spatial synchronization of unbalanced rotors excited with paralleled and counterrotating motors in a far resonance system. *J. Theor. Appl. Mech.* **2019**, *57*, 723–738. [CrossRef]
22. Jacazio, G.; Gastaldi, L. Equalization techniques for dual redundant electro hydraulic servo actuators for flight control systems. *Fluid Power Motion Control* **2008**, *2008*, 543–557.
23. Qi, H.; Mare, J.-C.; Fu, Y. Force equalization in hybrid actuation systems. In Proceedings of the 7th International Conference on Fluid Power Transmission and Control, Hangzhou, China, 7–10 April 2009; pp. 342–347.
24. Rehman, W.U.; Wang, S.; Wang, X.; Fan, L.; Shah, K.A. Motion synchronization in a dual redundant HA/EHA system by using a hybrid integrated intelligent control design. *Chin. J. Aeronaut.* **2016**, *29*, 789–798. [CrossRef]
25. Waheed, U.R.; Wang, S.; Wang, X.; Kamran, A. A position synchronization control for HA/EHA system. In Proceedings of the 2015 International Conference on Fluid Power and Mechatronics (FPM), Harbin, China, 5–7 August 2015; pp. 473–482.

26. Rehman, W.U.; Nawaz, H.; Wang, S.; Wang, X.; Luo, Y.; Yun, X.; Iqbal, M.N.; Zaheer, M.A.; Azhar, I.; Elahi, H. Trajectory based motion synchronization in a dissimilar redundant actuation system for a large civil aircraft. In Proceedings of the 2017 29th Chinese Control and Decision Conference (CCDC), Chongqing, China, 28–30 May 2017; pp. 5010–5015.
27. Rehman, W.U.; Wang, X.; Wang, S.; Azhar, I. Motion synchronization of HA/EHA system for a large civil aircraft by using adaptive control. In Proceedings of the 2016 IEEE Chinese Guidance, Navigation and Control Conference (CGNCC), Nanjing, China, 12–14 August 2016; pp. 1486–1491.
28. Rehman, W.U.; Wang, S.; Wang, X.; Shi, C.; Zhang, C.; Tomovic, M. Adaptive control for motion synchronization of HA/EHA system by using modified MIT rule. In Proceedings of the 2016 IEEE 11th Conference on Industrial Electronics and Applications (ICIEA), Hefei, China, 5–7 June 2016; pp. 2196–2201.
29. Wang, X.; Liao, R.; Shi, C.; Wang, S. Linear extended state observer-based motion synchronization control for hybrid actuation system of more electric aircraft. *Sensors* **2017**, *17*, 2444. [CrossRef] [PubMed]
30. Wang, X.; Shi, C.; Wang, S. Extended state observer-based motion synchronisation control for hybrid actuation system of large civil aircraft. *Int. J. Syst. Sci.* **2017**, *48*, 2212–2222. [CrossRef]
31. Ur Rehman, W.; Wang, X.; Cheng, Y.; Chai, H.; Hameed, Z.; Wang, X.; Saleem, F.; Lodhi, E. Motion synchronization for the SHA/EMA hybrid actuation system by using an optimization algorithm. *Automatika* **2021**, *62*, 503–512. [CrossRef]
32. Guo, L.L.; Yu, L.M.; Lu, Y.; Fan, D.L. Multi-mode switching control for HSA/EHA hybrid actuation system. In *Applied Mechanics and Materials*; Trans Tech Publications Ltd.: Bäch, Switzerland, 2014; pp. 1088–1093.
33. Rehman, W.U.; Khan, W.; Ullah, N.; Chowdhury, M.S.; Techato, K.; Haneef, M. Nonlinear Control of Hydrostatic Thrust Bearing Using Multivariable Optimization. *Mathematics* **2021**, *9*, 903. [CrossRef]
34. Rehman, W.U.; Wang, X.; Cheng, Y.; Chen, Y.; Shahzad, H.; Chai, H.; Abbas, K.; Ullah, Z.; Kanwal, M. Model-based design approach to improve performance characteristics of hydrostatic bearing using multivariable optimization. *Mathematics* **2021**, *9*, 388. [CrossRef]
35. Wang, S.; Tomovic, M.; Liu, H. *Commercial Aircraft Hydraulic Systems: Shanghai Jiao Tong University Press Aerospace Series*; Academic Press: Cambridge, MA, USA, 2015.
36. Wang, X.; Wang, S. Adaptive fuzzy robust control of PMSM with smooth inverse based dead-zone compensation. *Int. J. Control Autom. Syst.* **2016**, *14*, 378–388. [CrossRef]
37. Wang, L.; Maré, J.-C.; Fu, Y. Investigation in the dynamic force equalization of dissimilar redundant actuation systems operating in active/active mode. In Proceedings of the 28th International Congress of the Aeronautical Sciences ICAS 2012, Brisbane, Australia, 23–28 September 2012; p. session-6.8.1.
38. Wang, L.; Mare, J.-C.; Fu, Y.; Qi, H. Force equalization for redundant active/active position control system involving dissimilar technology actuators. In Proceedings of the 8th JFPS International Symposium on Fluid Power, Okinawa, Japan, 25–26 October 2011; pp. 136–143.
39. Elias, N.; Yahya, N. Simulation study for controlling direct current motor position utilising fuzzy logic controller. *Int. J. Automot. Mech. Eng.* **2018**, *15*, 5989–6000. [CrossRef]
40. Liu, X.; Wang, Y.; Wang, M. Speed Fluctuation Suppression Strategy of Servo System with Flexible Load Based on Pole Assignment Fuzzy Adaptive PID. *Mathematics* **2022**, *10*, 3962. [CrossRef]
41. Yin, H.; Yi, W.; Wu, J.; Wang, K.; Guan, J. Adaptive Fuzzy Neural Network PID Algorithm for BLDCM Speed Control System. *Mathematics* **2021**, *10*, 118. [CrossRef]